Environmental Toxicology and Pharmacology 99 (2023) 104086

Contents lists available at ScienceDirect

Environmental Toxicology and Pharmacology

journal homepage: www.elsevier.com/locate/etap

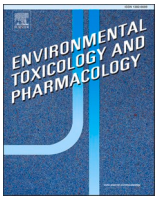

Enhancement of biological effects of oxidised nano- and microplastics in human professional phagocytes

Giuseppa Visalli [a], Antonio Laganà [a,b], Alessio Facciolà [a], Antonella Iaconis [a], Jessica Curcio [a], Santa Pollino [a], Consuelo Celesti [c], Silvia Scalese [d], Sebania Libertino [d], Daniela Iannazzo [c], Angela Di Pietro [a,*]

[a] Department of Biomedical and Dental Sciences and Morphofunctional Imaging, University of Messina, 98125 Messina, Italy
[b] Istituto Clinico Polispecialistico C.O.T. Cure Ortopediche Traumatologiche s.p.a., 98124 Messina, Italy
[c] Department of Electronic Engineering, Industrial Chemistry and Engineering, University of Messina, 98125 Messina, Italy
[d] Istituto per la Microelettronica e Microsistemi, Consiglio Nazionale delle Ricerche (CNR-IMM), Ottava Strada n.5, I-95121 Catania, Italy

ARTICLE INFO

Edited by Dr. M.D. Coleman

Keywords:
Nano and micro polystyrene particle
Uptake
Human monocyte
Macrophage-like cells
Environmental wear processes
Pro-oxidant effects

ABSTRACT

Micro and nanoplastics are ubiquitous pollutants that can cause adverse health effects even in humans. Effects of virgin and oxidised (simulating the aging processes) polystyrene nano (nPS) and micro particles (mPS) with diameters of 0.1 and 1 μm were studied on human professional phagocytes (i.e., monocyte cells THP-1 and macrophage-like mTHP-1 cells). After characterization by ATR-FTIR, UV-Vis spectroscopy, SEM and dynamic light-scattering analyses, the particles were FITC functionalised to quantify cellular uptake. Changes in the cell compartments were studied by acrydine orange and the pro-oxidant, cytotoxic and genotoxic effects were assessed. Phagocytosis was dose- and time- dependent and at 24 h 52% of nPS and 58% of mPS were engulfed. Despite the high homeostasis of professional phagocytes, significant ROS increases and DNA damage were observed after exposure to oxidised particles. The results highlight that the environmental aging processes enhances the adverse health effects of micro and nanoplastics.

1. Introduction

Plastic is one of the most widely produced materials in the contemporary era, thanks to its versatility of use and low production costs. The number of plastic items produced, of which 50% are disposable, is massive and a lot of plastic waste ends up in the environment. Here, they undergo fragmentation and partial degradation (aging processes), giving rise to secondary micro- and nanoplastics (Ter Halle et al., 2017; Luo et al., 2019, 2020; Paluselli et al., 2019). These particles, together with primary ones (Hirt and Body-Malapel, 2020; Domínguez-Jaimes et al., 2021), interact more easily with organisms, including humans, causing damage. The hazard of these emerging particulate pollutants lies in their hydrophobic nature which, favouring internalization, results in the capacity for bioaccumulation and biomagnification (Saley et al., 2019; Miller et al., 2020; Esposito et al., 2022).

In natural environments, the aging processes of plastics include mechanical abrasion, chemical oxidation—mainly due to ultraviolet (UV) radiation—and biodegradation (Liu et al., 2020), causing changes in the surface of plastic materials. As shown in polystyrene (PS) and polyvinyl chloride (PVC) irradiated with UV light, photo-oxidation increases the negative charges on the surface of plastics (Liu et al., 2019). The speed of photo-oxidative processes is directly proportional to the specific surface of the microplastics (Cooper and Corcoran, 2010). Furthermore, not all plastics have the same resistance to aging processes, and this seems to be influenced by both their nature and the chemical composition of the medium (Cooper and Corcoran, 2010; Zbyszewski and Corcoran, 2011).

The presence of microplastics (only the detectable) in different human body tissues, as well as their faecal excretion, has been established in several studies (Schwabl et al., 2019; Ibrahim et al., 2020; Amato-Lourenço et al., 2021; Braun et al., 2021; Ragusa et al., 2021;) To shed light on the potential pathogenesis of these particulate xenobiotics it is of paramount importance to assess their impact on human health. Recently, an increasing number of in vivo and in vitro studies have focused on this highly challenging issue, mainly evaluating the effects of virgin nano and micro polystyrene particles (Liu et al., 2022).

* Corresponding author.
E-mail address: angela.dipietro@unime.it (A. Di Pietro).

https://doi.org/10.1016/j.etap.2023.104086
Received 25 October 2022; Received in revised form 24 January 2023; Accepted 22 February 2023
Available online 24 February 2023

Polystyrene is not only among the most produced plastic polymers (Lambert and Wagner, 2016); Jeon et al. (2021)), it is also the one that best lends itself to evaluating its biological effects according to size, considering the commercial availability of nano- and micro-scale polystyrene beads. It is in fact the dimension that notoriously modulates the toxicity of particulate xenobiotics (Visalli et al., 2019). As size decreases, the reactivity of the particles increases due to the greater surface area to mass ratio (Trovato et al., 2018). Moreover, size regulates internalization and, consequently, the interaction with biological molecules (Banerjee et al., 2021; Paul et al., 2022). In an in vivo study on male Wistar rats, Wei et al. (2021) observed capillary congestion and myocardial fibre breakage after oral exposure to PS of 0.5 μm and 0.5 mm for 90 days. By using the same size of PS beads and the same route of exposure in male mice, Zhao et al. (2022) observed aorta inflammation and damage to perivascular adipose tissue. Several in vitro studies on different human cell lines confirmed the ability of nano and microplastic particles to cross cell membranes, causing oxidative damage, expression of inflammatory genes, changes in cell morphology, mitochondrial damage and genotoxicity (Zhu et al., 2020; Yu et al., 2022). To evaluate the detrimental effects of nanoplastic particles, Cortes et al. (2020) observed genotoxicity in cells of human colon adenocarcinoma (Caco-2), while Stock et al. (2019) confirmed the higher uptake of 1 μm microplastics in the same cells. An in vitro microfluidic study was used by Liu et al. (2022) to assess neurotoxicity of nano and micro polystyrene beads (0,1 and 1 μm) on mouse hippocampal neuronal HT22 cells. They observed cell cycle S phase arrest and adverse effects on cellular metabolism due to Reactive Oxygen Species (ROS) overproduction. However, the results are still fragmentary and sometimes conflicting and further studies are needed to fill the gaps for health risk assessment.

In humans, the innate defence system based on cells with phagocytic activity (the so-called professional phagocytes) acts to eliminate both abiotic and biotic foreign particles, which can reach the bloodstream and then penetrate different body districts (Uribe-Querol and Rosales, 2020).

Among the protagonists of this host response are monocytes and, above all, macrophages that present in various body tissues and differentiate from monocytes after chemotaxis-induced migration from the bloodstream. Both cell types play an essential role in inflammatory processes, producing cytokines such as tumour necrosis factor (TNF-alpha) and interleukin-6 (IL-6) (Friedlander et al., 1994; Boraschi et al., 2017). Their pivotal roles in the clearance of invaders and innate immune response processes makes it essential to study damage induced by nano- and microplastics in these cells for the purpose of plastic-induced pathogenesis assessment.

To this aim, after evaluating uptake we performed an in vitro study to examine the pro-oxidant, cytotoxic and genotoxic effects of polystyrene particles with 0.1 μm (nPS) and 1 μm (mPS) diameter on the human monocyte cell line THP-1 and, after differentiation, on macrophage-like cells (mTHP-1). Like other researchers (Shi et al., 2021; Liu et al., 2022; Paul et al., 2022), we selected these sizes to assess size-induced effects as the most representative of micro- and nanoparticles, respectively. To better reproduce actual exposure conditions, in addition to virgin particles, both cell types were exposed to oxidised particles, simulating environmental aging processes. The increased reactivity of aged nano- and microplastics promotes interactions with biomolecules and cells in exposed organisms, including humans. This suggests an enhancement of adverse health effects, still poorly studied in human cells. Therefore, the main goal of our study was to assess the biological effects induced by wear processes by comparing between virgin and oxidised nPS/mPS.

2. Materials and methods

2.1. Virgin and oxidised nPS and mPS

The tested virgin mPS (v-mPS) and nPS (v-nPS) consisted of PS with a diameter of 1 μm and 0.1 μm (Sigma-Merck, Milan, Italy; code: BCC8557 and BCC9279). Prior to each experiment, stock suspensions (10 mg mL^{-1}) were prepared in phosphate buffer saline (PBS; pH 7.4) that, after appropriate dilution, were put in contact with the assayed cells. The stock suspensions were also subjected to oxidation by treatment at 80 °C for 2 h to obtain the oxidised mPS (ox-mPS) and nPS (ox-nPS) samples (Mielczarski et al., 2011). This step allowed the presence of carboxyl, alkoxyl and hydroxyl groups on the particle surface. The presence of oxygen-containing groups was detected using a Fourier-Transform Infrared (FT-IR) Spectra by Two FT-IR Spectrometers (PerkinElmer Inc., Waltham, Massachusetts, U.S) by ATR method in the range of 4000–500 cm^{-1}. Size measurements were performed by dynamic light-scattering (DLS) analyses using the Zetasizer 3000 instrument (Malvern, Worcestershire, UK), equipped with a 632 nm HeNe laser, operating at a 173-degree detector angle (Iannazzo et al., 2019).

The scanning electron microscopy (SEM) analysis was performed using a Supra 35 FE-SEM (Zeiss, Oberkochen, Germany) to compare the size and shape of v-nPS/mPS and ox-nPS/mPS.

To further characterize all samples, UV-Vis spectra were recorded using a UV-Vis spectrophotometer (Cary® 50 UV/vis by Agilent Technologies, Santa Clara, CA, U.S) in a wavelength range between 200 and 800 nm, using wide optical window quartz cuvettes (200–2500 nm).

To quantify cellular uptake spectrofluorometrically, the ox-nPS and ox-mPS (i.e., functionalised plastic particles) were covalently bound to fluorescein isothiocyanate (FITC), which was in turn bound to a polyethylene glycol (PEG) linker containing two amino groups, one of which was protected with a *tert*-butyloxycarbonyl (Boc) group. The reaction between one of the amino groups of the PEG linker and FITC was carried out at room temperature in dichloromethane and in the presence of triethylamine.

The solvent was removed and the product was characterised by Fourier-transform infrared (FTIR) spectroscopy. After deprotection of the Boc group, the FITC-PEG system was conjugated to oxidised PS particles via a coupling reaction using 1-ethyl-3-(3-dimethylaminopropyl) carbodiimide (EDC) and hydroxybenzotriazole (HOBt) as coupling reagents. The reaction was carried out in dimethylformamide (DMF) after removing most of the aqueous solution from the PS suspensions. The conjugation took place by allowing the mixture to stir at room temperature for four days. To eliminate FITC not bound to particles, solvent and other by-products of the reaction, the suspensions were dialysed against distilled H_2O until organic material was no longer detectable in the dialysis fluid (5 days). The complexes were then analysed by FTIR spectroscopy using a Spectrum Two FT-IR Spectrometer.

2.2. Cell cultures

The THP-1 cell line (ATCC: TIB-202), a human cell line derived from a patient with acute monocytic leukemia, was used as a biological model. The cells were grown in the culture medium RPMI 1640 supplemented with 2 mM of L-glutamine, 10 mM of HEPES, 1 mM of pyruvate sodium, 0.05 mM of 2-mercaptoethanol, 2.5 g L^{-1} of glucose, 10% (v/v) of foetal bovine serum (FBS), 100 UI mL^{-1} of penicillin and 100 μg mL^{-1} of streptomycin in a humidified atmosphere containing 5% CO_2 at 37 °C. The cells, which were morphologically roundish, were grown in suspension and subcultures were set up when the density was equal to 9×10^5 mL^{-1}.

THP-1 cells were also differentiated to macrophage-like cells (mTHP-1) by cultivating them in a M-SFM medium with the addition of 200 nM of phorbol myristate acetate (PMA) for 48 − 72 h in a humidified atmosphere containing 5% CO_2 at 37 °C (Currò et al., 2014).

2.3. Uptake of nPS/mPS

To evaluate uptake spectrofluorometrically, THP-1 cells were differentiated to macrophages in 96-well plates and then treated with 20 and 40 μg mL^{-1} of nPS-FITC/mPS-FITC suspensions in culture medium with 2% FBS (100 μl/well; 8 wells per sample). After 1, 3 and 24 h, fluorometric readings were carried out at the excitation and emission wavelengths of 485 nm and 535 nm, respectively, using a microplate reader (Tecan Italia, Milan, Italy). After recording the emission values in each well, the medium was removed, the monolayer was repeatedly washed with PBS, and emission values were recorded to measure the percent uptake (i.e., intracellular nPS-FITC/mPS-FITC).

The uptake was confirmed by microscope observation using a CLSM equipped with a 40 × 1.0 NA immersion objective and TCS SP2 instrument (Leica Microsystem Heidelberg, Mannaheim, Germany).

2.4. Evaluation of cellular compartments

To assess the effects of nPS/mPS uptakes in cellular compartments, we stained the treated cells with cell-permeable acrydine orange (AO). The metachromatic fluorophore allows the study of changes in endocytic apparatus (i.e., mature endosomes or phagolysosomes and lysosomes) (Trybus et al., 2017). Thanks to the proton pump, AO is remarkably sequestered, emitting a red fluorescence in the acidic compartment. Conversely, AO releases a green fluorescence in the cytosol and in the nucleus where it is present at lower concentrations. When AO binds in monomeric form to the DNA double helix, it emits a green fluorescence while a very low green emission indicates DNA denaturation. Therefore, an intense localized red signal indicates a consistent internalization in the intact acidic compartment, while the loss of the red and green fluorescence indicates cellular injuries in acidic and nuclear compartments. In the experiments, the THP-1 cells, differentiated and not, were exposed to virgin and oxidised nano- and microplastics at 100 μg mL^{-1} for 3 h.

To analyse the microscopic fields, we used ImageJ software (imagej.nih.gov/ij/index.htm) that allowed us to calculate the emitted red and green fluorescence for each treated cell (at least 100 cells) and the respective ratio, and compare the values to those recorded in the control cells (PBS treated).

2.5. Assessment of ROS production

The pro-oxidant effect of virgin and oxidised nPS and mPS was evaluated measuring the production of reactive oxygen species (ROS) on THP-1 cells and mTHP-1 cells using the 2',7'-dichlorofluorescein-diacetate probe (DCF-DA) (Sigma-Merck, Milan-Italy).

Briefly, in 96-well microplates with 5 × 10^5 cell mL^{-1}, the probe solution, at a concentration of 1 μM, prepared in PBS solution containing 10 mM D-glucose at pH 7.4, was added and microplates were incubated at 37 °C for 30 min. Next, the probe solution was removed and the cells were treated with virgin and oxidised n-PS and m-PS at concentrations of 100 μg mL^{-1} in maintenance medium for the times described in the experimental protocol. In addition to control cells, cells treated with 300 μM of H_2O_2 were used as positive controls. The fluorometric reading was performed by a microplate reader at excitation and emission wavelengths of 485 nm and 535 nm, respectively. Fluorescence values, expressed in arbitrary fluorescence units (AFUs), were used to calculate percentage changes (%Δ) with respect to control cells (Di Pietro et al., 2011; Visalli et al., 2015).

2.6. Assessment of DNA damage

A comet assay was used to assess DNA damage on both undifferentiated and differentiated THP-1, exposed for 24 h to v-nPS/mPS and ox-nPS/mPS, suspensions (100 μg mL^{-1}). Samples, PBS- treated cells and positive controls (cells treated with 300 μM of H_2O_2) were run in duplicate on ~2 × 10^4 cells for each spot, and electrophoresis was carried out using a Hercules power supply set to 300 mA and 25 V (0.86 V cm^{-1}). The slides, stained with ethidium bromide (20 μg mL^{-1}), were imaged using a DMIRB fluorescence microscope (Leica Microsystems) equipped with a digital camera (Power Shot S50; Canon, Milan, Italy) at 400 × total magnification (Micale et al., 2013). The analysis was carried out in at least 100 nuclei per slide using the CASP software (Comet assay software project, http://casp.sourceforge.net). The percentage of DNA in the tail (% TDNA) was considered as the parameter of DNA damage.

2.7. Viability assays

In both cell types, the v-nPS/mPS and ox-nPS/mPS cytotoxicity was evaluated in the range of 25–100 μg mL^{-1}. In the THP-1 suspended cells the analysis was performed after 24 h using a propidium iodide (PI) solution (3 μg mL^{-1}) both without cell permeabilization (dead cells) and after methanol treatment (viable cells with intact plasma membrane). The cell suspensions were fluorometrically measured using 535 and 615 nm as excitation and emission wavelengths and the percentage of dead cells was calculated from the ratio of the emission value of the non-permeabilized suspension to the total emission value (non-permeabilized + permeabilized suspensions). The colorimetric MTT assay, based on the reduction of 3-(4,5-dimethiazol-2)− 2,5-difeniltetrazolium bromide, was used to assess cytotoxicity in mTHP-1 cells. A preliminary abiotic test, which was performed to assess the eventual reduction of MTT by the particle surface, ruled out this event. Briefly, the appropriate volume of the stock suspension of v-nPS/mPS and ox-nPS/mPS was added to the cells differentiated for 24 h in 96-well microplates. After 24 h, using the standard protocol, MTT was added and after incubation at 37 °C, the enzymatic activity of viable cells was quantified by spectrophotometric measurement at 540 nm using a microplate reader (Tecan Italia, Milan- Italy).

2.8. Statistical analyses

All data are presented as the mean ± standard deviation (SD) based on at least three independent experiments. After verifying that for each parameter examined the data distribution was Gaussian by the Lilliefor's and Shapiro–Wilk normality tests ($p > 0.05$), the data were analysed by one-way analysis of variance (ANOVA) (GraphPad Prism 8). The relationships between different parameters were assessed using the Pearson correlation coefficient. Significance was accepted at $p < 0.05$.

2.9. Oxidation and characterization of nPS and mPS

To simulate the aging processes to which nPS/mPS are subjected in the environment, we oxidised virgin plastic particles. Heat treatment in PBS has shown to trigger swelling processes and structural changes in the polymer. Due to their large molecular size, adsorbed phosphate ions promote relaxation of the polymer chain, favouring the light-mediated oxidative cleavage processes. The methylene groups present on the benzene rings of the polymer surface undergo structural modifications involving the formation of peroxidic intermediates, which then lead to the formation of hydroxyl, carbonyl and carboxylic compounds. The formed ox-nPS and ox-mPS were characterized by ATR-FTIR spectroscopy to evaluate the presence of oxygen containing groups (Fig. 1). The FTIR spectrum of ox-nPS (Fig. 1A) shows a peak at 3020 cm^{-1} due to the stretching vibration of the C−H bond of the aromatic groups, together with a peak at 2910 cm^{-1}, due to the stretching of C−H bonds of the methylene groups. The wide band at ~3500 − 3000 cm^{-1} was ascribable to the stretching vibration of the O−H groups present in the polymer following the fragmentation process. This broad band was much more intense in the oxidised material due to the increased number of oxygenated functionalities after treatment with PBS. In the oxidised sample, there was also an intense peak at 1660 cm^{-1} attributable to the increased presence of carboxyl groups and a peak at 1058 cm^{-1}

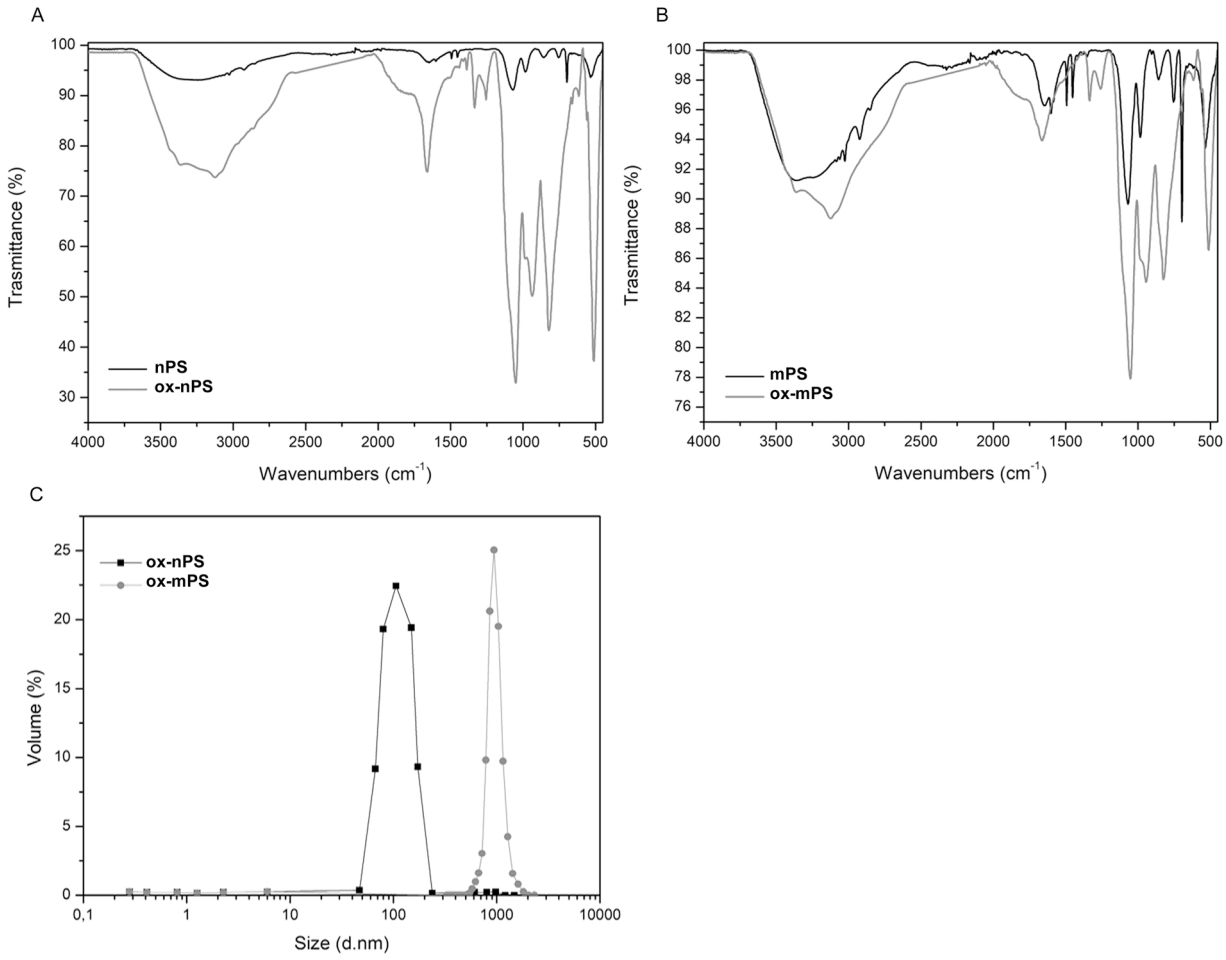

Fig. 1. nPS(mPS characterization. (A) FTIR spectra of v-nPS and ox-nPS; (B) FTIR spectra of v-mPS and ox-mPS. (C) Volume weighted size distributions of ox-nPS and ox-mPS samples. FTR spectra were obtained in sample suspensions performed in deionized water at concentrations of 0.1 mg mL-1.

attributable to the stretching of the C−O bond of the alkoxy groups. In a similar way, the oxidation of mPS led to the formation of the same oxygen-containing functional groups (Fig. 1B) with increased intensities with respect to the starting material.

We also investigated whether after oxidative treatment the particles' sizes changed as a result of possible aggregations. Dynamic light-scattering DLS analyses allowed us to confirm that the average size of the microplastics remained unchanged, suggesting that functionalisation occurred only at the surface of the particles and it did not cause aggregation of the particles, either in the suspensions in PBS or in those in cell medium. The weighted size distributions for ox-nPS and ox-mPS samples of 108 nm and 909 nm, respectively, were observed (Fig. 1C).

Some changes in morphology and size after the oxidation process were observed by SEM analysis in mPS. Scanning electron microscopy images of nPS and mPS are reported in Fig. 2 (A, B, C) and in Fig. 2 (D, E, F), respectively. The ox-mPS showed an irregular surface and different size values while the ox-nPS remained almost unchanged, both in size and shape. A size increase was observed (1.2 μm) in only a negligible fraction (~10%) of ox-mPS, while it was, on average, 0.85 μm in the others. These data confirm the results obtained from DLS analyses where almost superimposable results of particles size for virgin and oxidised nano- or microplastics have been recorded.

UV-Vis spectra (Fig. 2G, H) highlighted a marked increase in the entire absorbance signal after the oxidation process of both nPS and mPS which, had different spectra. Unlike ox-nPS, for the ox-mPS sample, a shoulder in the visible absorption region can be clearly observed. This shoulder, which became relatively stronger after the oxidation process, can be due to the different light scattering effect of the particles. In particular, with a concentration of 0.2 mg mL^{-1}, a peak at 231 nm and a large feature between 250 nm and 270 nm were observed for mPS. For the same concentration value of ox-mPS, the absorbance signals in the visible range increased and both the peak at 231 nm and the large feature between 250 nm and 270 nm became more intense and defined, underlining the increased presence of oxygen-containing functional groups on the particle surface. The peak series between 230 and 270 nm can be related to the phenyl groups (lower wavelengths) and to oxygenated functionalities such as carbonyl and phenol functionalities (higher wavelengths), as also confirmed by FTIR spectra.

A different absorbance spectrum was observed for nPS (concentration of 0.1 mg mL^{-1}), showing peaks in the UV range between 200 and 225 nm and almost no absorbance in the visible range. A lower concentration was used for nPS with respect to mPS due to a very intense signal in the UV region reaching the saturation limit of the detector. This was done after verifying that the shape of the nPS spectra for 0.2 mg/mL^{-1} and 0.1 mg/mL^{-1} was identical in the whole wavelength range. For ox-nPS (Fig. 2G), a marked intensification of the peaks between 200 and 225 nm (that are not shown in larger particles) is observed and there is still no absorbance peak in the visible region. The peak at 204 nm can be attributable to the absorbance of the aromatic carboxyl groups, while the absorbance at 216 and 225 nm can be related to the π-π * transition of the sp^2 carbon-conjugated system and the presence of carbonyl and phenol groups on ox-nPS particles after heat treatment with PBS. All these absorption peaks are more intense in the oxidised sample with respect to its precursor due to the increased presence of oxygen functionalities, as also reported by FTIR characterization. The lack of shoulder in the visible region of the UV spectrum is due to the

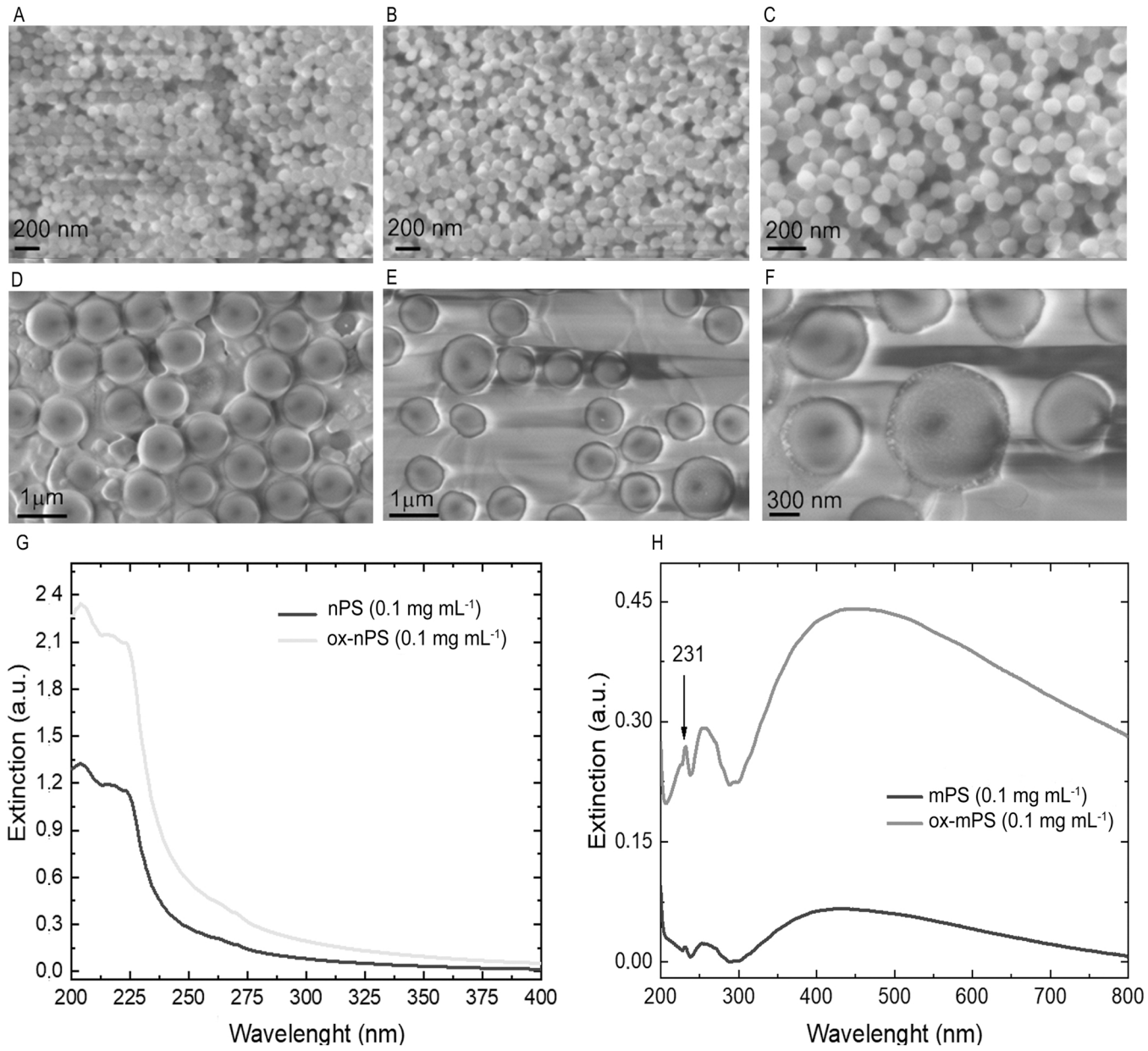

Fig. 2. nPS(mPS characterization. SEM analysis of (A) v-nPS (B) ox-nPS; (C) ox-nPS at higher magnification; (D) v-mPS; (E) ox-nPS; (F) ox-nPS at higher magnification. Virgin and oxidised nPS/mPS were suspended in PBS. (G) UV-Vis absorption spectra acquired on PBS solutions containing v- and ox-nPS and (H) containing v- and ox-mPS.

nanometric size of these particles, which, as also confirmed by DLS analysis, have no tendency to aggregate in water solution and do not produce significative light scattering.

2.10. FITC conjugation of nPS/mPS

Covalent binding of FITC with ox-nPS and ox-mPS was achieved using a PEG moiety containing two amino groups as the bidentate linker, one of which was protected with a Boc group (PEG-NH_2) (Fig. 3A). The free amino group present in the linker was used to form a thiourea linkage with FITC. The conjugated compound was subsequently deprotected at the amine functionality to give the FITC-PEG-NH_2 sample containing a free amino group. The FTIR spectrum of FITC-PEG-NH_2, compared with the starting FITC, highlighted the synthesis of the compound, which is necessary for the conjugation of the nPS/mPS. We confirmed the amide bond formation between nPS and mPS and FITC. We evaluated the PL properties of the FITC-conjugated samples, nPS-FITC and mPS-FITC, in deionised water after irradiation at the excitation wavelength of 380 nm by comparing their PL spectra with those of the starting FITC and ox-nPS and ox-mPS (Fig. 3B, C). The PL spectra of nPS-FITC sample showed a distinct emission peak at 512 nm while for the mPS-FITC sample, a peak at 516 nm was recorded (Fig. 3B). For both oxidized samples no relevant fluorescence emission was recorded. These spectra demonstrate the effective fluorescence of the polystyrene nano- and microplastics conjugated with fluorescein. After conjugation with the fluorescent tracer, DLS analyses showed unchanged volume-weighted size distributions in comparison to ox-nPS and ox-mPS samples.

2.11. Internalisation of nPS and mPS

To quantify the phagocytosis of nPS/mPS, we performed a time course on macrophage-like cells using nPS-FITC and mPS-FITC suspensions at concentrations of 20 and 40 µg mL^{-1} (i.e., 2 and 4 µg per well),

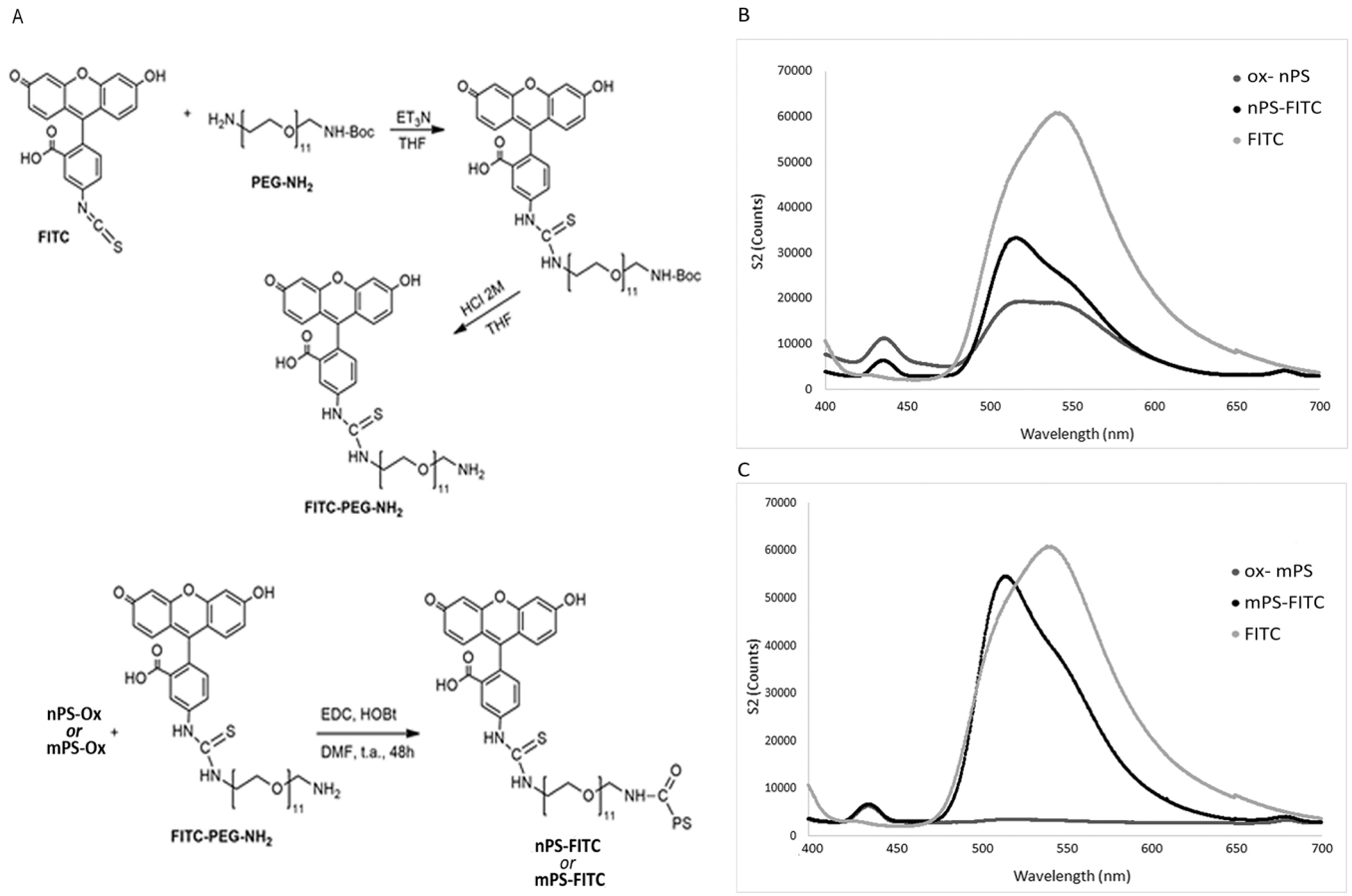

Fig. 3. Synthesis and characterization of nPS/mPS- FITC. (A) Step-by-step synthesis of nPS- and mPS-FITC. (B) PL spectra of nPS-FITC and (C) of mPS-FITC. In the PL spectra of mPS-FITC sample a peak at 516 nm was recorded. For both the oxidized samples no relevant fluorescence emission was recorded. The spectra further confirm the presence of a covalent bond between FITC and the polymers since a shift was observed in the conjugates with respect to the starting FITC. The observed bathochromic effect is indicative of the stable interaction between nPS/mPS and FITC.

for 1, 3 and 24 h. Preliminary abiotic tests showed that the emission values (expressed in arbitrary fluorescence units [AFU] in the experimental conditions were 72.45 and 97.13 for 1 μg of nPS and mPS, respectively, confirming the higher peak shown by mPS-FITC in the PL spectra. The internalized μg was calculated by measuring the emission values in mTHP-1 after discharging the medium and repeatedly washing with PBS to evaluate the engulfed particles exclusively. The time course of particle phagocytosis was dose- and time- dependent for both particle sizes with no significant differences between the two sizes (Fig. 4A). For both particles, the kinetics of nPS/mPS uptake indicated that the internalisation process was extremely rapid and 21% and 27% of mPS and nPS, respectively, were engulfed after only 1 h of exposure to the

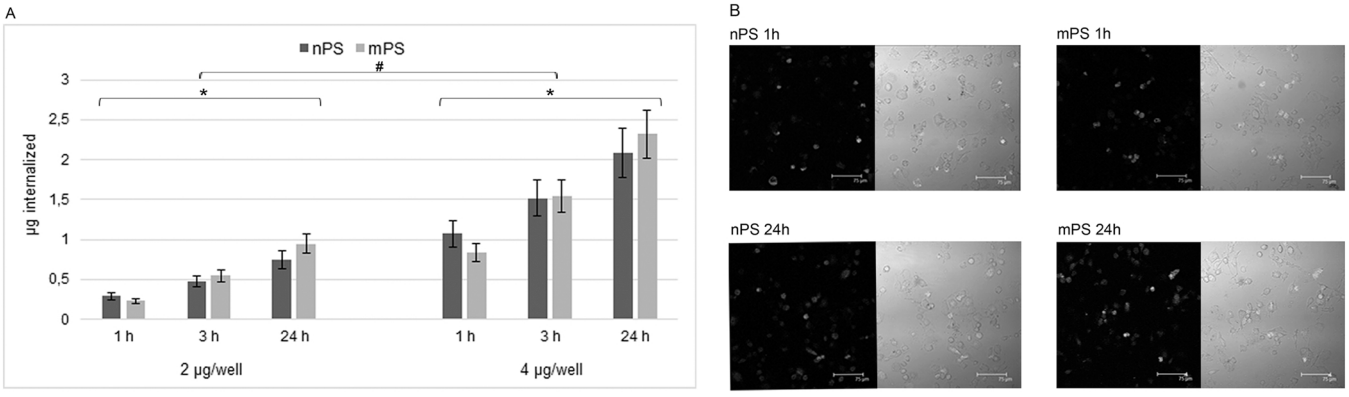

Fig. 4. Particle phagocytosis on macrophage-like cells using suspensions of nPS/mPS-FITC at concentrations of 20 and 40 μg mL^{-1} (2 and 4 μg/well) for 1, 3 and 24 h. (A) Time course of nPS/mPS phagocytosis; the graph reports for each μg/well the average (± SD) of the internalised particles. The particle phagocytosis was dose- and time- dependent for both particle sizes without differences between the two sizes (*p* value not significant), while significant dose# and time * differences were observed for both nPS and mPS by ANOVA test. A significant relationship exposure-time was also observed to Pearson test. (B) Representative images confirm the intracellular nPS-FITC/mPS-FITC, respectively, and show a diffuse green florescence in most of the treated mTHP-1, which was more marked in mPS-FITC-treated cells.

highest dose. At 24 h, these percentages increased further, at least doubling, and as many as 52% and 58% corresponding to 2.08 and 2.32 μg per well of nPS and mPS, respectively, were engulfed (Pearson correlation coefficient [r] > 0.95 and 0.97, respectively; $p < 0.05$). Although there was a greater efficiency of macrophages in phagocytising larger particles, albeit with a greater delay, we cannot exclude that this was caused by a leakage of nPS over time. Considering the density and the size of PS particles, we calculated a difference in number of internalised particles equal to three orders of magnitude per μg internalised. With the same mass engulfed, the markedly higher number of internalised nPS highlighted the greater surface area developed by the last particles.

The confocal laser scanning microscopy (CLSM) analyses confirmed the intracellular nPS-FITC/mPS-FITC and showed a diffuse and marked green florescence in most of the treated mTHP-1 (Fig. 4B).

2.12. Effect of virgin and oxidised nPS and mPS on the cellular compartments

Changes in the endocytic apparatus (late endosomes and lysosomes), as well as in the nuclear compartment, were examined by employing AO in THP-1 cell suspensions and in semi-confluent mTHP-1 monolayers, grown in chamber slides. Both cell types were treated for 3 h with 100 μg mL^{-1} of v-nPS/mPS and ox-nPS/mPS (Fig. 5A, B for THP-1 and mTHP-1, respectively).

The analysis of THP-1 cells revealed an intact and increased acid compartment in cells treated with v-nPS/mPS, a clear indication that these particles—after phagocytosis—did not determine an evident permeabilization of phagolysosomes. Compared to the control cells, which showed a ratio of red/green emissions of 0.424 (±0.05), this was 0.569 (±0.08) and 0.623 (±0.06) for v-nPS and v-mPS with a %Δ equal to 34.2 and 46.7, respectively. Conversely, in THP-1 treated with ox-nPS/mPS, apparently there was no clear evidence of internalization in acidic compartments and, compared to virgin-treated, the ones treated with ox-nPS/mPS had significantly decreased red fluorescence, underlining the leakage of lysosomal content ($p < 0.05$ and $p<0.01$ in ox-nPS and ox-mPS, respectively), as shown in CLSM images (Fig. 5C). In the mTPH-1 cells a significant reduction in both red and green emitted fluorescence was observed. Regardless of the size and type of particles (virgin and/or oxidised), in the treated mTHP-1, the values of red and green fluorescence were on average halved in comparison to the control cells ($p < 0.05$) (Fig. 5B and D).

2.13. Reactive oxygen species production by nPS and mPS

The time course (1–24 h) of reactive oxygen species (ROS) production, expressed as %Δ compared to control cells, in THP-1 cells and mTHP-1 cells treated with v-nPS/mPS and ox-nPS/mPS (100 μg mL^{-1}) are reported (Fig. 6A, B for THP-1 and mTHP-1, respectively). As expected, in both cell types, the ROS production was rather contained, underlining the remarkable ROS neutralization capacity of these cells and confirmed by the average content of %Δ values calculated in the positive control (H_2O_2 treated cells) that were 15.5 and 7.6 in THP-1 and mTHP-1, respectively. In particular, exposure to v-nPS/mPS showed no difference in TPH-1 cells compared to the control cells. Despite a good homeostatic ability in the short term, starting at 3 h, in THP-1 cells exposed to ox-nPS/mPS the values were almost comparable to the positive control. The different pro-oxidant effect of oxidised particles compared to virgin ones was also observed in mTHP-1 cells treated with nanoplastics; although, virgin nPS/mPS also caused oxidative stress in

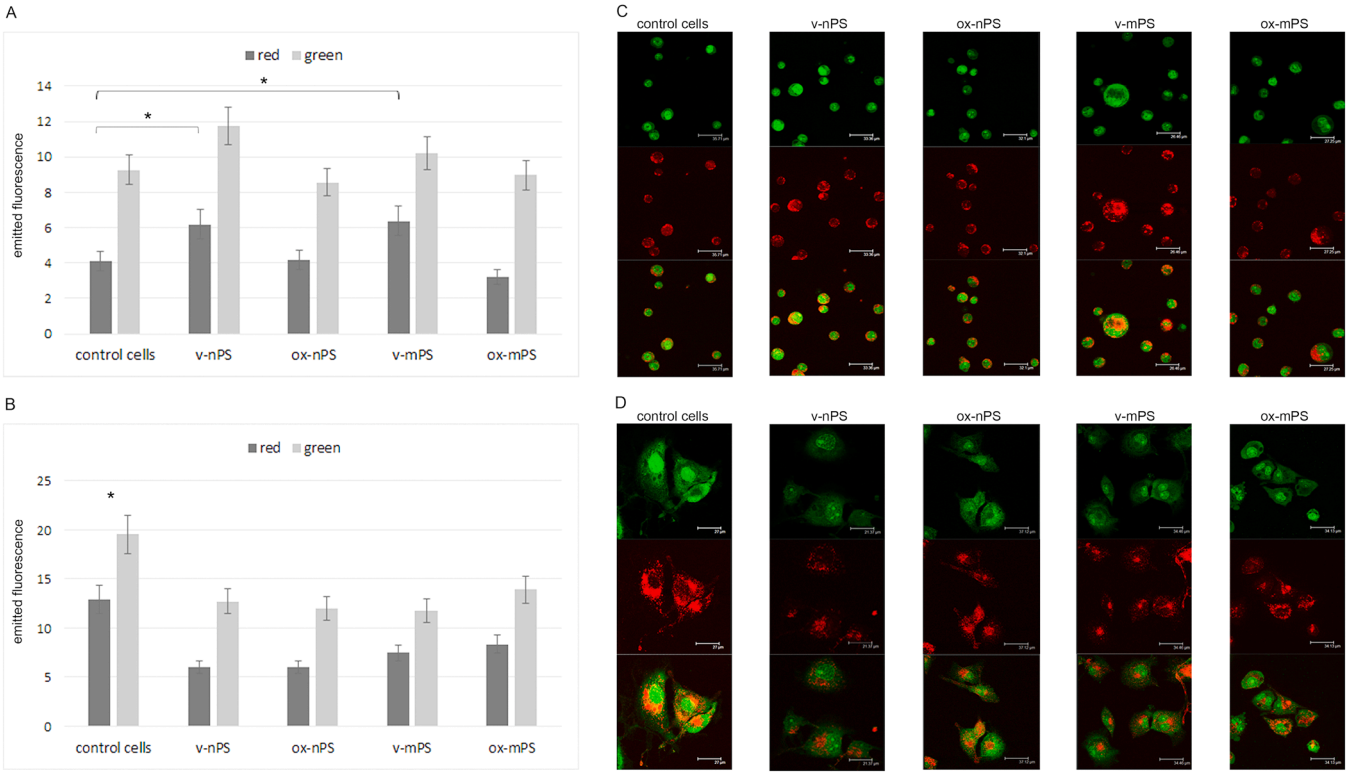

Fig. 5. Results of CLSM analyses by employing AO to evaluate endocytic apparatus (red emitted fluorescence) and nuclear compartment (green emitted fluorescence) after treatment for 3 h with v- and ox-nPS and mPS (100 μg mL^{-1}). (A) results of THP-1 cell suspension. In comparison to control cells significant differences were observed in red fluorescence emission of v-nPS and v-mPS treated cells ($p < 0.05$). (B) results of semi-confluent mTHP-1monolayers. In comparison to control cells significant differences in red and green fluorescence emissions were observed in nPS/mPS treated cells ($p < 0.05$). (C) THP-1 cells. The graphs report the average (± SD) of emitted fluorescence (expressed in arbitrary units of fluorescence AFU) recorded by ImageJ software in at least 50 cells. The significance was assessed by ANOVA test (D) Representative CLSM images of mTHP-1 cells.

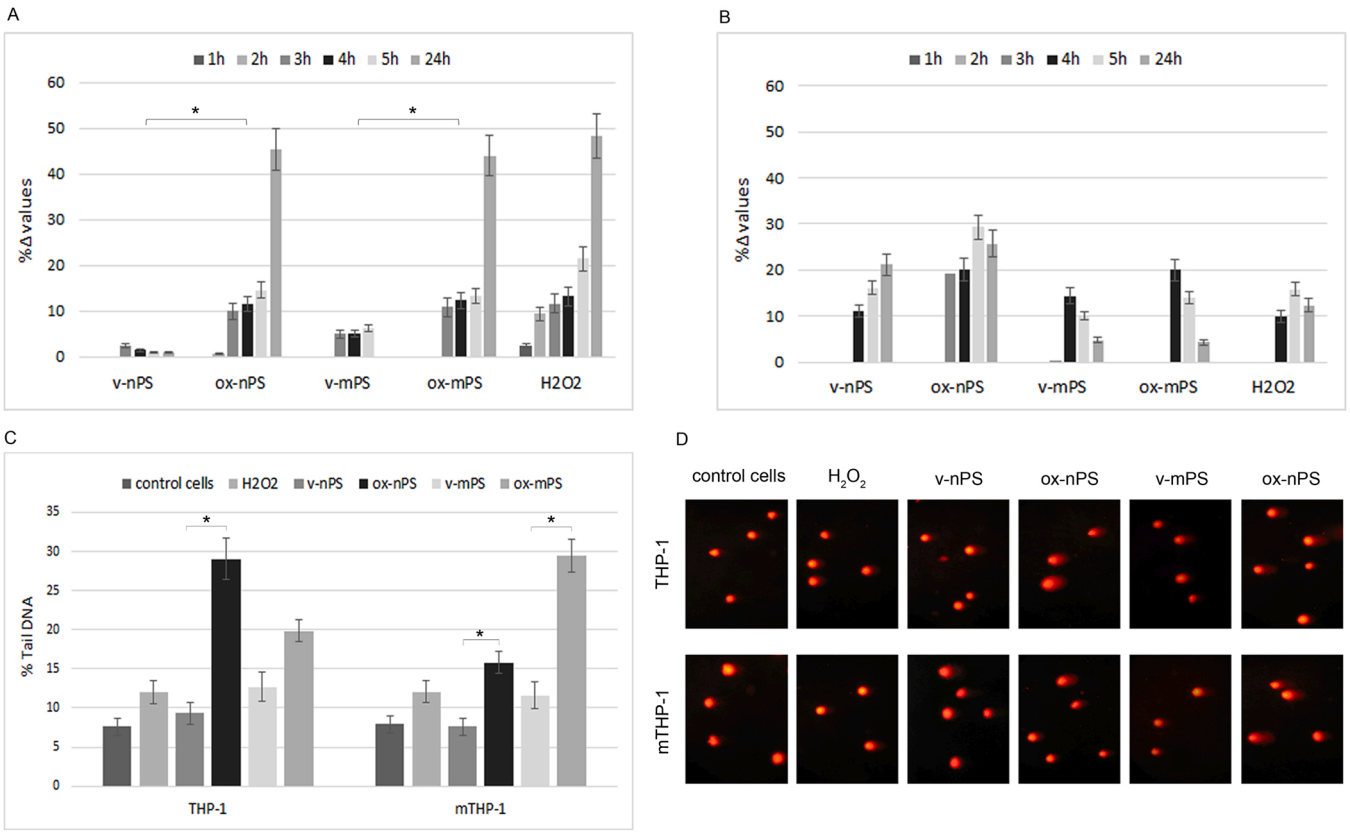

Fig. 6. ROS production and Comet assay results in cells treated with v- and ox-nPS/mPS (100 μg mL−1). (A) Time course (1–24 h) of ROS production in THP-1 cell suspensions. *In comparison to v-nPS/mPS, the ox-nPS/mPS caused significant ROS overproduction ($p < 0.05$). (B) Time course (1–24 h) of ROS production in semi-confluent mTHP-1 cells. The values are expressed as %Δ compared to control cells and fluorometric analysis was performed using the probe DCF-DA. Cells treated with 300 μM of H2O2 were used as a positive control. The significance was assessed by ANOVA test. (C) DNA damage assessed by the Comet assay after exposure for 24. *In THP-1 ox-nPS caused a significant increase of %TDNA in comparison to v-nPS ($p < 0.05$). *In mTHP-1 oxidised nPS/mPS caused significant increases of % TDNA in comparison to the virgin counterparts ($p < 0.05$). The graphs report the average ± SD of %TDNA values recorded in at least 100 nuclei per sample. The significance was assessed by ANOVA test. (D) Representative images of the cells treated and analysed by the Comet assay.

these cells. In particular, the average %Δ in v-nPS treated mTHP-1 was completely comparable to the positive control (7.5 vs. 7.6) to double then in cells treated with ox-nPS ($p < 0.05$) while the values were comparable between v-mPS and ox-mPS.

2.14. Genotoxic damage induced by nPS and mPS

The comet test, whose results are reported in Fig. 6C and D for each cell type, was used to verify genotoxic damage in cells exposed to both v-nPS/mPS and ox-nPS/mPS. Even in these experiments, the values of the positive control underlined the remarkable antioxidant equipment of professional phagocytes to counteract oxidative DNA damage (in both cell types, 12 was the %TDNA value in H_2O_2 treated cells). However, despite this, the ox-nPS/mPS induced significant damage that was diversified both in function of the two types of cells and of the particles. In fact, in monocytes, the highest value was observed after exposure to ox-nPS (%TDNA 29.0), 2.4-fold in comparison to the positive control ($p < 0.01$). In macrophage-like cells, ox-mPS caused greater DNA damage (%TDNA 29.4; $p < 0.01$), underlining the more marked reactivity of ox-nPS/mPS.

2.15. Cytotoxicity induced by nPS and mPS

In both assayed cell types, the above reported effects caused a rather moderate cytotoxicity at 24 h, confirming the remarkable homeostasis capabilities of these cells, the first line of defence against foreign particles. In THP-1 and mTHP-1 cells, treated with v-nPS/mPS at the highest dose (100 μg mL^{-1}), the percentages of dead cells were nearly overlapping those observed in control cells. No differences were observed between v-nPS and v-mPS and the percentages were 3.9 and 3.1 in THP-1 and mTHP-1 cells, respectively. A slight increase in dead cells was observed in the ones treated with ox-nPS/mPS whose values always remained below 10%. The moderate cell death nPS/mPS induced confirmed the high homeostasis of professional phagocytes even though the experiment to assess changes in cellular compartments in the short exposure time (2 h) highlighted substantial damages to both the acidic compartment and the nucleus with potential denaturation of the DNA.

3. Discussion

The potential adverse health effects of nano- and microplastics in humans are still poorly evaluated and studies focusing on the health effects of aged nano- and microplastics subjected to environmental wear processes are almost absent. In addition to mechanical fragmentation due to winds and the erosive action of wave motion, which allows internalization of nano- and microplastics into biological system, photo- and thermo-chemical oxidation increases the negative charges on the surfaces of plastics, enhancing their reactivity (Veerasingam et al., 2016; Song et al., 2017; Liu et al., 2019, 2020). However, most in vitro studies on human cell lines evaluated the effects of virgin spherical PS particles. Only Zhu et al. (2020) and Yu et al. (2022) studied the effects of photo-oxidised plastic particles in human lung epithelial (A549) and intestinal epithelial (Caco-2) cells, observing an increased cytotoxicity in comparison to virgin particles due to ROS overproduction. More

recently, Volkl et al. (2022) performed a careful and in-depth analysis on mammalian cells using the murine ImKC cell line (Kupffer cells) to assess the effects of mPS with different degrees of photo-oxidation. The results showed higher pro-oxidant effects induced by photo-oxidised mPS. Overall, these few studies confirmed our results and highlighted that, for a more realistic risk assessment, it is essential to resort to oxidised nano- and microplastics, which are the most representative component of these ubiquitous pollutants, subjected in the environment to progressive wear. On this basis, the main goal of our study was to compare the effects induced by oxidised nPS/mPS to those induced by virgin plastics, which are more studied (Visalli et al., 2021).

We preliminarily characterized nPS/mPS artificially subjected to oxidation according to Mielczarski et al. (2011). Using ATR-FTIR and UV-Vis spectroscopy, we verified the consistent increase of oxygen-containing groups on the surface of both PS particles after the oxidation process. Similar to what observed after photo-oxidation (Hebner and Maurer-Jones, 2020), our ox-mPS sample showed an increase in the visible absorption region with respect to its precursor that can be rationalised by hydrogen bond interaction and the oxygen containing group present in the microparticles after the oxidative process. As reported by Kato et al. (2009) and Wang et al. (2020), the absorption increase was stronger for the larger particles than for the smaller ones. The study of photo-oxidative degradation occurring during artificial aging was also performed by Biale et al. (2021). Like us, they reported the surface-limited formation of oxidised aromatic structures in PS particles without involvement of the overall polymer mass. Carbonyl and phenol functionalities detected by FTIR spectra were also observed by Li et al. (1991).

The presence of functional groups on the particle surface considerably increases the reactivity of the particles and as expected, our study also highlights the greater damage induced by aged particles compared to virgin ones, similar to what was reported by almost all previous studies (Zhu et al., 2020; Völkl et al., 2022; Yu et al., 2022).

However, it is necessary to add that the biological effects of aged plastics are also a function of the environmental matrix in which they are dispersed. In fact, the presence of dissolved organic matter could neutralize the greater surface reactivity by the adsorption process, as observed by Schür et al. (2021).

Because the diameter, as well as the surface characteristics, regulate the effects of the particles by modifying their bioavailability, using SEM and DLS analyses we could rule out significant changes in particle sizes due to aggregation after artificial aging.

Using homemade FITC-loaded nPS/mPS, we quantified the uptake and highlighted the speed and the efficiency by which both nPS and mPS were internalised in our cell models. In professional phagocytes the main pathway of particle internalisation is endocytosis. However, for nPS we cannot exclude that there is also an energy-independent diffusion process, exclusively regulated by the chemical gradient. Passive diffusion, i.e., crossing of the phospholipid bilayer, is highly favoured by the hydrophobicity that characterises plastics, enhancing their bioavailability (Saley et al., 2019; Miller et al., 2020), and it is only partially counteracted by the frictional coefficient of the particle related to the viscosity of the medium and the interactions between particles and macromolecules diluted in the solvent (Trovato et al., 2018).

The remarkable and innate ability of professional phagocytes to internalise foreign particles was dose- and time- dependent, with no significant differences based on particle size. However, the surface changes in ox-nPS/mPS played a pivotal role in the intracellular localisation of particles, modulating the interaction with cellular macromolecules and organelles in monocytes and macrophage-like cells respectively. The stepwise process of endocytosis consists of particle and/or macromolecule internalization through vesicles derived from the plasma membrane and involves GTPases for actin polymerisation (Kumari et al., 2010). The early endosomes merge with lysosomes to form phagolysosomes (late endosomes) where degradative enzymes are activated thanks to vesicle acidification. While monocytes treated with v-nPS/mPS showed an intact and increased acidic compartment, where the virgin particles were seized, the ox-nPS/mPS would seem to escape endosomes. Although this could be attributed to phagolysosomal permeabilization, with leakage of lysosomal content producing irreversible cytoplasmic acidification, enzymolysis and apoptosis (i.e., the Trojan horse effect) (Trovato et al., 2018), we would rule it out. Cytotoxicity, although greater in ox-nPS/mPS than the virgin counterpart, was moderate, making it plausible to believe that oxidised plastic particles escape early from the endosomes (before their fusion with lysosomes) and they randomly localise in the cell cytoplasm, causing the observed ROS overproduction and genotoxicity.

The differences between v-nPS/mPS and ox-nPS/mPS were not observed in macrophage-like cells for which, regardless of aging and size, the escape from endosomes always occurred, as shown by the decreased emission of red fluorescence in cells stained by the AO probe. Surprisingly, in treated mTHP-1 cells in comparison to control cells we also observed in a short time (2 h) the decrease of green fluorescence. It will be necessary to further investigate this behaviour which, considering the low cytotoxicity observed at 24 h, does not seem to be irreversible and due to DNA denaturation. Plausibly, it could be due to the greater unwinding of the DNA double helix to allow expression of the genes necessary to counteract the damage induced by nPS/mPS and trigger innate immunity, such as the production of pro-inflammatory cytokines.

A further goal of the study was to detect the biological effects of nPS/mPS on the cells assigned to implement the mechanisms of innate defence to counteract any damage caused by foreign biotic and abiotic particles to which humans can be exposed. Despite the remarkable homeostasis capabilities of these cells, the results highlight the harmful effects induced by artificially aged nPS/mPS. Professional phagocytes can counteract the etiological agents of infection even with the so-called “oxidative burst” in addition to phagolysosomal digestion. The event due to NADPH oxidase activation produces superoxide and H_2O_2 with antimicrobial activity; therefore, these cells are equipped with a rich antioxidant kit to prevent oxidation of its own biomolecules, as confirmed by the results obtained in the positive control consisting of 300 μM H_2O_2 treated cells. Despite this, oxidized nPS/mPS caused ROS overproduction higher in THP-1 than in mTHP-1, potentially triggering pathogenic processes affecting professional phagocytes, as well as genotoxicity, clearly demonstrated by the Comet test. Our results disagree with what Jeon et al. (2021) reported on mTPH-1. Compared to virgin microplastics, they observed a lower cytotoxicity in the ones photodegraded which was attributed to the neutralization of the reactive plastic surface by serum proteins (corona effect).

The pathogenic mechanisms induced by other nano- and microparticles, both natural (combustion by-products) and synthetic (metal- and carbon-based nanomaterials) are far more powerful than those reported in this study for nPS/mPS (Visalli et al., 2017, 2019). However, it is necessary to consider that the quantities of the latter to which individuals are exposed are massive and destined to increase, thanks to the progressive aging of plastics incorrectly and constantly discarded in the environment.

4. Conclusions

Unlike v-nPS/mPS, whose effects were rather limited, our results highlighted the considerable pro-oxidant potential of plastic particles that have undergone oxidative degradation. Despite the rich antioxidant kit of professional phagocytes, the efficient and fast uptake of ox-nPS/mPS caused ROS overproduction, which in turn was responsible for DNA damage and increased cytotoxicity. All this confirmed the enhancement of the biological effects induced by the wear processes hypothesised by us. Since oxidation is the most important degradation process to which plastics undergo during their aging in the environment, our results indicate the poor utility of in vitro studies using virgin microplastics to assess the impact of these ubiquitous pollutants on

human health. Moreover, the observed effects in the examined cell models could trigger systemic pathogenic processes considering the role played by innate immunity cells in the inflammatory cascade. We therefore intend to investigate the pro-inflammatory effects of these pollutants in the near future.

Funding

This research did not receive any specific grant from funding agencies in the public, commercial, or not-for-profit sectors.

CRediT authorship contribution statement

GV: Validation, Formal analysis, Investigation. **AL:** Formal analysis, Investigation. **AF:** Formal analysis, Investigation. **AI:** Resources. **JC:** Resources. **SP:** Resources. **CC:** Chemical analyses. **SS:** Chemical analyses. **SL:** Chemical analyses. **DI:** Chemical analyses. **ADP:** Conceptualization, Methodology, Writing and Supervision text.

Declaration of Competing Interest

The authors declare that they have no known competing financial interests or personal relationships that could have appeared to influence the work reported in this paper.

Data Availability

Data will be made available on request.

References

Amato-Lourenço, L.F., Carvalho-Oliveira, R., Júnior, G.R., Dos Santos Galvão, L., Ando, R.A., Mauad, T., 2021. Presence of airborne microplastics in human lung tissue. J. Hazard. Mater. 416, 126124 https://doi.org/10.1016/j.jhazmat.2021.126124.

Banerjee, A., Billey, L.O., Shelver, W.L., 2021. Uptake and toxicity of polystyrene micro/nanoplastics in gastric cells: Effects of particle size and surface functionalization. PLoS One 16 (12), e0260803. https://doi.org/10.1371/journal.pone.0260803.

Biale, G., La Nasa, J., Mattonai, M., Corti, A., Vinciguerra, V., Castelvetro, V., Modugno, F.A., 2021. Systematic study on the degradation products generated from artificially aged microplastics. Polymers 13 (12), 1997. https://doi.org/10.3390/polym13121997.

Boraschi, D., Italiani, P., Palomba, R., Decuzzi, P., Duschl, A., Fadeel, B., Moghimi, S.M., 2017. Nanoparticles and innate immunity: new perspectives on host defence. Semin Immunol. 34, 33–51. https://doi.org/10.1016/j.smim.2017.08.013.

Braun, T., Ehrlich, L., Henrich, W., Koeppel, S., Lomako, I., Schwabl, P., Liebmann, B., 2021. Detection of microplastic in human placenta and meconium in a clinical setting. Pharmaceutics 13 (7), 921. https://doi.org/10.3390/pharmaceutics13070921.

Cooper, D.A., Corcoran, P.L., 2010. Effects of mechanical and chemical processes on the degradation of plastic beach debris on the island of Kauai, Hawaii. Mar. Pollut. Bull. 60 (5), 650–654. https://doi.org/10.1016/j.marpolbul.2009.12.026.

Cortes, C., Domenech, J., Salazar, M., Pastor, S., Marcos, R., Hernandez, A., 2020. Nanoplastics as a potential environmental health factor: effects of polystyrene on human intestinal epithelial Caco-2 cells 2020. Environ. Sci.: Nano 7 (1), 272–285. https://doi.org/10.1039/C9EN00523D.

Currò, M., Ferlazzo, N., Risitano, R., Condello, S., Vecchio, M., Caccamo, D., Ientile, R., 2014. Transglutaminase 2 and phospholipase A_2 interactions in the inflammatory response in human Thp-1 monocytes. Amino Acids 46 (3), 759–766. https://doi.org/10.1007/s00726-013-1569-y.

Di Pietro, A., Baluce, B., Visalli, G., La Maestra, S., Micale, R., Izzotti, A., 2011. Ex vivo study for the assessment of behavioral factor and gene polymorphisms in individual susceptibility to oxidative DNA damage metals-induced. Int. J. Hyg. Environ. Health 214 (3), 210–218. https://doi.org/10.1016/j.ijheh.2011.01.006.

Domínguez-Jaimes, L.P., Cedillo-González, E.I., Luévano-Hipólito, E., Acuña-Bedoya, J. D., Hernández-López, J.M., 2021. Degradation of primary nanoplastics by photocatalysis using different anodized TiO2 structures. J. Hazard. Mater. 413, 125452 https://doi.org/10.1016/j.jhazmat.2021.125452.

Esposito, G., Prearo, M., Renzi, M., Anselmi, S., Cesarani, A., Barcelò, D., Dondo, A., Pastorino, P., 2022. Occurrence of microplastics in the gastrointestinal tract of benthic by-catches from an eastern Mediterranean deep-sea environment. Mar. Pollut. Bull. 174, 113231 https://doi.org/10.1016/j.marpolbul.2021.113231.

Friedlander, M.A., Hilbert, C.M., Wu, Y.C., Finegan, C.K., Rich, E.A., 1994. Disparate cytochemical characteristics and production of cytokines and prostaglandin E2 by human mononuclear phagocytes from the blood, lung, and peritoneal cavity. J. Lab. Clin. Med. 123, 574–584.

Hebner, T.S., Maurer-Jones, M.A., 2020. Characterizing microplastic size and morphology of photodegraded polymers placed in simulated moving water conditions. Environ. Sci. Process. Impacts 22, 398–407. https://doi.org/10.1039/C9EM00475K.

Hirt, N., Body-Malapel, M., 2020. Immunotoxicity and intestinal effects of nano- and microplastics: a review of the literature. Part Fibre Toxicol. 17, 57. https://doi.org/10.1186/s12989-020-00387-7.

Iannazzo, D., Pistone, A., Celesti, C., Triolo, C., Patané, S., Giofré, S.V., Romeo, R., Ziccarelli, I., Mancuso, R., Gabriele, B., Visalli, G., Facciolà, A., Di Pietro, A., 2019. A smart nanovector for cancer targeted drug delivery based on graphene quantum dots. Nanomaterials 9, 282. https://doi.org/10.3390/nano9020282.

Ibrahim, Y.S., Tuan Anuar, S., Azmi, A.A., Wan Mohd Khalik, W.M.A., Lehata, S., Hamzah, S.R., Ismail, D., Ma, Z.F., Dzulkarnaen, A., Zakaria, Z., Mustaffa, N., Tuan Sharif, S.E., Lee, Y.Y., 2020. Detection of microplastics in human colectomy specimens. JGH Open 5 (1), 116–121. https://doi.org/10.1002/jgh3.12457.

Jeon, S., Lee, D.K., Jeong, J., Yang, S.I., Kim, J.S., Kim, J., Cho, W.S., 2021. The reactive oxygen species as pathogenic factors of fragmented microplastics to macrophages. Environ. Pollut. 281, 117006 https://doi.org/10.1016/j.envpol.2021.117006.

Kato, H., Nakamura, A., Takahashi, K., Kinugasa, S., 2009. Size effect on UV-Vis absorption properties of colloidal C (60) particles in water. Phys. Chem. Chem. Phys. 11 (25), 4946–4948. https://doi.org/10.1039/b904593g.

Kumari, S., Mg, S., Mayor, S., 2010. Endocytosis unplugged: multiple ways to enter the cell. Cell Res. 20 (3), 256–275. https://doi.org/10.1038/cr.2010.19.

Lambert, S., Wagner, M., 2016. Formation of microscopic particles during the degradation of different polymers. Chemosphere 161, 510–517. https://doi.org/10.1016/j.chemosphere.2016.07.042.

Li, T., Zhou, C., Jiang, M., 1991. UV absorption spectra of polystyrene. Polym. Bull. 25, 211–216. https://doi.org/10.1007/BF00310794.

Liu, P., Qian, L., Wang, H., Zhan, X., Lu, K., Gu, C., Gao, S., 2019. New insights into the aging behavior of microplastics accelerated by advanced oxidation processes. Environ. Sci. Technol. 53 (7), 3579–3588. https://doi.org/10.1021/acs.est.9b00493.

Liu, P., Zhan, X., Wu, X., Li, J., Wang, H., Gao, S., 2020. Effect of weathering on environmental behavior of microplastics: Properties, sorption and potential risks. Chemosphere 242, 125193. https://doi.org/10.1016/j.chemosphere.2019.125193.

Liu, S., Li, Y., Shang, L., Yin, J., Qian, Z., Chen, C., Yang, Y., 2022. Size-dependent neurotoxicity of micro- and nanoplastics in flowing condition based on an in vitro microfluidic study. Chemosphere 303 (3), 135280. https://doi.org/10.1016/j.chemosphere.2022.135280.

Luo, H., Zhao, Y., Li, Y., Xiang, Y., He, D., Pan, X., 2020. Aging of microplastics affects their surface properties, thermal decomposition, additives leaching and interactions in simulated fluids. Sci. Total Environ. 714, 136862 https://doi.org/10.1016/j.scitotenv.2020.136862.

Luo, W., Su, L., Craig, N.J., Du, F., Wu, C., Shi, H., 2019. Comparison of microplastic pollution in different water bodies from urban creeks to coastal waters. Environ. Pollut. 246, 174–182. https://doi.org/10.1016/j.envpol.2018.11.081.

Micale, R.T., La Maestra, S., Di Pietro, A., Visalli, G., Baluce, B., Balansky, R., Steele, V.E., De Flora, S., 2013. Oxidative stress in the lung of mice exposed to cigarette smoke either early in life or in adulthood. Arch. Toxicol. 87 (5), 915–918. https://doi.org/10.1007/s00204-012-0993-1.

Mielczarski, J.A., Jeyachandran, Y.L., Mielczarski, E., Rai, B., 2011. Modification of polystyrene surface in aqueous solutions. J. Colloid Interface Sci. 362 (2), 532–539. https://doi.org/10.1016/j.jcis.2011.05.068.

Miller, M.E., Hamann, M., Kroon, F.J., 2020. Bioaccumulation and biomagnification of microplastics in marine organisms: A review and meta-analysis of current data. PLoS One 15, e0240792. https://doi.org/10.1371/journal.pone.0240792.

Paluselli, A., Fauvelle, V., Galgani, F., Sempéré, R., 2019. Phthalate release from plastic fragments and degradation in seawater. Environ. Sci. Technol. 53 (1), 166–175. https://doi.org/10.1021/acs.est.8b05083.

Paul, M.B., Fahrenson, C., Givelet, L., Hermann, T., Loeschner, K., Böhmert, L., Thünemann, A.F., Braeuning, A., Sieg, H., 2022. Beyond microplastics – investigation on health impacts of submicron and nanoplastic particles after oral uptake in vitro. Microplastics Nanoplastics 2, 16. https://doi.org/10.1186/s43591-022-00036-0.

Ragusa, A., Svelato, A., Santacroce, C., Catalano, P., Notarstefano, V., Carnevali, O., Papa, F., Rongioletti, M.C.A., Baiocco, F., Draghi, S., D'Amore, E., Rinaldo, D., Matta, M., Giorgini, E., 2021. Plasticenta: first evidence of microplastics in human placenta. Environ. Int. 146, 106274 https://doi.org/10.1016/j.envint.2020.106274.

Saley, A.M., Smart, A.C., Bezerra, M.F., Burnham, T.L.U., Capece, L.R., Lima, L.F.O., Carsh, A.C., Williams, S.L., Morgan, S.G., 2019. Microplastic accumulation and biomagnification in a coastal marine reserve situated in a sparsely populated area. Mar. Pollut. Bull. 146, 54–59. https://doi.org/10.1016/j.marpolbul.2019.05.065.

Schür, C., Weil, C., Baum, M., Wallraff, J., Schreier, M., Oehlmann, J., Wagner, M., 2021. Incubation in wastewater reduces the multigenerational effects of microplastics in daphnia magna. Environ. Sci. Technol. 55 (4), 2491–2499. https://doi.org/10.1021/acs.est.0c07911.

Schwabl, P., Köppel, S., Königshofer, P., Bucsics, T., Trauner, M., Reiberger, T., Liebmann, B., 2019. Detection of various microplastics in human stool: a prospective case series. Ann. Intern. Med. 171, 453–457. https://doi.org/10.7326/M19-0618.

Shi, Q., Tang, J., Wang, L., Liu, R., Giesy, J.P., 2021. Combined cytotoxicity of polystyrene nanoplastics and phthalate esters on human lung epithelial A549 cells and its mechanism. Ecotoxicol. Environ. Saf. 213, 112041 https://doi.org/10.1016/j.ecoenv.2021.112041.

Song, Y.K., Hong, S.H., Jang, M., Han, G.M., Jung, S.W., Shim, W.J., 2017. Combined effects of UV exposure duration and mechanical abrasion on microplastic fragmentation by polymer type, 18 Environ. Sci. Technol. 51 (8), 4368–4376. https://doi.org/10.1021/acs.est.6b06155.

Stock, V., Bohmert, L., Lisicki, E., Block, R., Cara-Carmona, J., Pack, L.K., Selb, R., Lichtenstein, D., Voss, L., Henderson, C.J., Zabinsky, E., Sieg, H., Braeuning, A., Lampen, A., 2019. Uptake and effects of orally ingested polystyrene microplastic particles in vitro and in vivo. Arch. Toxicol. 93, 1817–1833. https://doi.org/10.1007/s00204-019-02478-7.

Ter Halle, A., Ladirat, L., Martignac, M., Mingotaud, A.F., Boyron, O., Perez, E., 2017. To what extent are microplastics from the open ocean weathered? Environ. Pollut. 227, 167–174. https://doi.org/10.1016/j.envpol.2017.04.051.

Trovato, M.C., Andronico, D., Sciacchitano, S., Ruggeri, R.M., Picerno, I., Di Pietro, A., Visalli, G., 2018. Nanostructures: between natural environment and medical practice. Rev. Environ. Health 33 (3), 295–307. https://doi.org/10.1515/reveh-2017-0036.

Trybus, W., Król, T., Trybus, E., Kopacz-Bednarska, A., Król, G., Karpowicz, E., 2017. Changes in the lysosomal system of cervical cancer cells induced by emodin action. Anticancer Res. 37 (11), 6087–6096. https://doi.org/10.21873/anticanres.12057.

Uribe-Querol, E., Rosales, C., 2020. Phagocytosis: our current understanding of a universal biological process. Front. Immunol. 11, 1066. https://doi.org/10.3389/fimmu.2020.01066. ⟨https://doi.org/10.3389/fimmu.2020.01066⟩.

Veerasingam, S., Saha, M., Suneel, V., Vethamony, P., Rodrigues, A.C., Bhattacharyya, S., Naik, B.G., 2016. Characteristics, seasonal distribution and surface degradation features of microplastic pellets along the Goa coast, India. Chemosphere 159, 496–505. https://doi.org/10.1016/j.chemosphere.2016.06.056.

Visalli, G., Baluce, B., Bertuccio, M., Picerno, I., Di Pietro, A., 2015. Mitochondrial-mediated apoptosis pathway in alveolar epithelial cells exposed to the metals in combustion-generated particulate matter. J. Toxicol. Environ. Health A 78 (11), 697–709. https://doi.org/10.1080/15287394.2015.1024081.

Visalli, G., Facciolà, A., Iannazzo, D., Piperno, A., Pistone, A., Di Pietro, A., 2017. The role of the iron catalyst in the toxicity of multi-walled carbon nanotubes (MWCNTs). J. Trace Elem. Med. Biol. 43, 153–160. https://doi.org/10.1016/j.jtemb.2017.01.005.

Visalli, G., Facciolà, A., Currò, M., Laganà, P., La Fauci, V., Iannazzo, D., Pistone, A., Di Pietro, A., 2019. Mitochondrial impairment induced by sub-chronic exposure to multi-walled carbon nanotubes. Int J. Environ. Res. Public Health 16 (5), 792. https://doi.org/10.3390/ijerph16050792.

Visalli, G., Facciolà, A., Pruiti Ciarello, M., De Marco, G., Maisano, M., Di Pietro, A., 2021. Acute and sub-chronic effects of microplastics (3 and 10 μm) on the human intestinal cells HT-29. Int J. Environ. Res. Public Health 18 (11), 5833. https://doi.org/10.3390/ijerph18115833.

Völkl, M., Jérôme, V., Weig, A., Jasinski, J., Meides, N., Strohriegl, P., Scheibel, T., Freitag, R., 2022. Pristine and artificially-aged polystyrene microplastic particles differ in regard to cellular response. J. Hazard. Mater. 435, 128955 https://doi.org/10.1016/j.jhazmat.2022.128955.

Wang, X., Li, Y., Zhao, J., Xia, X., Shi, X., Duan, J., Zhang, W., 2020. UV-induced aggregation of polystyrene nanoplastics: Effects of radicals, surface functional groups and electrolyte. Environ. Sci.: Nano 7, 3914–3926. https://doi.org/10.1039/D0EN00518E.

Wei, J., Wang, X., Liu, Q., Zhou, N., Zhu, S., Li, Z., Li, X., Yao, J., Zhang, L., 2021. The impact of polystyrene microplastics on cardiomyocytes pyroptosis through NLRP3/Caspase-1 signaling pathway and oxidative stress in Wistar rats. Environ. Toxicol. 36 (5), 935–944. https://doi.org/10.1002/tox.23095.

Yu, X., Lang, M., Huang, D., Yang, C., Ouyang, Z., Guo, X., 2022. Photo-transformation of microplastics and its toxicity to Caco-2 cells. Sci. Total Environ., 150954 https://doi.org/10.1016/j.scitotenv.2021.150954.

Zbyszewski, M., Corcoran, P.L., 2011. Distribution and degradation of fresh water plastic particles along the beaches of Lake Huron, Canada. Water Air Soil Pollut. 220, 365–372. https://doi.org/10.1007/s11270-011-0760-6.

Zhao, J., Gomes, D., Jin, L., Mathis, S.P., Li, X., Rouchka, E.C., Bodduluri, H., Conklin, D. J., O'Toole, T.E., 2022. Polystyrene bead ingestion promotes adiposity and cardiometabolic disease in mice. Ecotoxicol. Environ. Saf. 232, 113239 https://doi.org/10.1016/j.ecoenv.2022.113239.

Zhu, K., Jia, H., Sun, Y., Dai, Y., Zhang, C., Guo, X., Wang, T., Zhu, L., 2020. Enhanced cytotoxicity of photoaged phenol-formaldehyde resins microplastics: combined effects of environmentally persistent free radicals, reactive oxygen species, and conjugated carbonyls. Environ. Int. 145, 106137 https://doi.org/10.1016/j.envint.2020.106137.